Nanoplasmonic Pyramidal Metamaterial Absorber at Optical Frequencies

Muhammad Amin (masharif@taibahu.edu.sa)
Taibah University https://orcid.org/0000-0002-1913-8451
Saleh Abdullah Basamed
Taibah University
Ahmed Salem Qniqoon
Taibah University
Faisal Aied Alshabibi
Taibah University
Saleh Mohammed Ba Raean
Taibah University
Hamad Edhah Aldhlea
Taibah University

Research Article

Keywords: Metamaterials, Plasmonics, Absorbers, Solar cells, Energy harvesting

Posted Date: January 5th, 2022

DOI: https://doi.org/10.21203/rs.3.rs-1229468/v1

Abstract

A pyramidal shaped metamaterial absorber (PMA) supports broadband and polarization independent resonant absorption at optical frequencies. The PMA is designed by stack of alternative plasmonic/dielectric multilayers. These nanoplasmonic pyramids offers resonant absorption characteristics at wide range of optical frequencies. The optimized PMA structure allows 76% spectral absorption and nearly perfect absorption (over 90%) at several bands between range of 400 nm – 1500 nm wavelength. These light absorption characteristics of PMA are useful for photodetection, thermal imaging, thermal emitters, and solar cells etc.

Introduction

Electromagnetic (EM) wave absorbers is the synthesized materials that can prevent the scattering of electromagnetic fields. Electromagnetic (EM) field absorbers can be divided into two categories based on their mode of operation i.e., resonant and broadband absorbers [1]. Resonant absorbers depend on the material interrelating with the incident waves in a resonant fashion around certain frequency [2, 3, 4]. There are two scientists who independently created similar devices, who developed EM absorbers are W. W. Salisbury and J. Jaumann [5, 6]. One of these devices, known as the Salisbury screen was first demonstration of resonant absorber. The resonant electromagnetic field absorber are based on crossed grating structure that make uses a reflective metal sheet having an engraved shallow periodic framework [7, 8]. On the other hand, the wideband absorbers depend on special materials whose characteristics are largely independent of electromagnetic frequency. Ideally such materials are well suited for this purpose that can contribute to inhibition of scattering of electromagnetic radiation over a wideband of frequencies [2]. Absorbers based on geometric transition are commonly used in anechoic chambers. Such absorbers can be categorized as broadband electromagnetic wave absorber. Another type of a broadband absorber, known as the sparse density absorber that relies on a very hollow materials so that its fill-factors can mostly be approximated nearly those of free space [1].

Recently, there is emphasis in scientific community to design efficient metamaterial-based absorbers. Metamaterials are the specialized structures with characteristic properties which are not found in nature [9]. These are synthesized with existing materials providing invisible properties in the nature, such as negative refraction [10, 11], perfect absorption, and resonant induced transmission [12, 13]. Metamaterials can be applied to various field domains such as perfect lenses [14, 15], chiral surfaces [16, 17], transformational surface [18], optical cloaking [19], spatial light switching [20, 21] and IR camouflage and microwave antennas because of the certain useful characteristics [2]. In addition to other applications, the perfect metamaterial absorber (PMA) that can efficiently absorb electromagnetic wave with meta-materials provide tremendous near field enhancements to improve the performance of solar cells [22], plasmonic sensor [23], thermal emitter and thermal image, photo-detectors [24].

Electromagnetic metamaterials (MMs) can be described as an effective medium and characterized by properties such as complex electric permittivity (ε) and magnetic permeability (μ) [25]. Much of the work

in MMs has been focused on the real part of ε and μ, as it contributes to negative refraction etc. It is important to reduce losses and represented by the imaginary part of ε and μ [26, 27] for practical applications related with wave propagation. On the other hand, absorbers rely on material losses to induce absorption. Lately, a thin metamaterial absorber (MA) have been projected by Landy et al., wherein electromagnetic resonance enables the MA to achieve matched impedance to free space [27]. The impedance is matching between effective medium forming metasurface with dielectric and background medium frequently free space, rejecting the reflection and efficiently absorbing the incident EM wave [27, 28].

Several MAs have been attracted significant attention from microwave to optical frequencies [29, 30]. However, the absorption bandwidth is frequently narrow due to the resonant nature of MAs. To overcome this problem, the MA units resonate at numerous adjacent frequencies to extend the absorption bandwidth [31, 32]. Generally, the metamaterial absorbers are composed of a patterned metal film overhead a continuous thin metallic film with a dielectric substrate sandwiched in between them [33, 34, 4, 8]. There are several reports on the extension of absorption bandwidth, however the bandwidth of the absorption still narrow [31], and in several studies the absorption spectrum is distributed to discrete absorption ranges [32].

Plasmonic metamaterial absorbers can also be used to harvest sunlight energy [22]. As the sunlight consists of spectrum ranging from ultraviolet, visible, infrared frequencies and it is often important to tap all the spectrum to fully benefit from the solar energy. Typically, the sun radiation consists of electromagnetic energy between a range of frequencies known as the Solar Spectrum [35]. Within this range the irradiance at different frequency varies i.e., sunlight energy irradiance is approximately 2% UV, 47% visible and 51% infra-red [36]. On the other hand, the shorter wavelength offers corresponding higher electromagnetic energy [37]. A plasmonic metamaterials absorber must be equipped to efficiently utilize all this energy source [39].

In this work, a pyramid metamaterial absorber (PMA) are proposed to provide wideband absorption at optical frequencies. The total absorption is dependent on resonances induced in the nanoplasmonic metasurface and the resonant interference between neighboring reflectors. The interference effects due to the multilayer metasurface are optimized to achieve wideband absorption of light at optical frequencies. The proposed multilayer absorber offers potential for several applications including solar cell energy harvesting, sensing, photodetectors etc.

Pma Structure

The design illustration of the PMA is shown in Fig. 1, consisting of periodic array of quadrangular frustum pyramids on top of a continuous planar metal film as the ground layer to prevent the fields in the forward direction. A unit cell of a periodic array is consists of multilayer nanoplasmonic metallic-dielectric quadrangular frustum pyramids. The sample of PMA is composed of five metal/dielectric layers with a thickness of 10 nm each. The width of each layer increases linearly from the top to the bottom. Each two

adjacent metal layers are separated by a dielectric spacer layer with the relative permittivity of 4.4. The metallic nanolayer is composed of gold. The optical properties of gold material are interpolated from experimental data reported by Johnson Christy [38]. The patch size with parameters Wt and W_l of PMA mainly dominates the resonance frequency, and the thickness of the dielectric spacer t_d controls resonance interference. The ground of PMA is considered as a homogeneous metallic film of enough large thickness to prevent the transmission of EM waves. The dimensions of the pyramid shown in Fig. 1 are t_d = 10 nm, t_m = 10 nm, P =100 nm, W_l = 90 nm, W_t = 50 nm, and the total thickness T = 100 nm (unless stated otherwise). A plane wave is normally incident on the PMA structure polarized along the x-axis having direction of propagation along -z direction. The four-fold symmetry of the structure allows the response of PMA polarization independent.

Simulation Modeling

The simulation of the PM A structure is performed by a Full wave electromagnetic simulation software. In the simulation setup, periodic boundary conditions are used in the x and y directions, and the incident and reflected fields are calculated at port defined along vertical direction along z-axis.

Electromagnetic (EM) wave impinging on a PMA can be described as transmitted T(λ), reflected R(λ), or absorbed A(λ), which are associated with the energy conservation law:

$$\mathrm{T}(\lambda) + \mathrm{R}(\lambda) + \mathrm{A}(\lambda) = 1$$

1

which T(λ), R(λ), and A(λ) are transmissivity, reflectivity, and absorptivity as functions of wavelength λ, respectively.

From the equation (1) we can calculate the absorption as A(λ) = 1 - T(λ) - R(λ). Since the ground is a thick layer of gold, therefore $T(\lambda) = |S_{21}(\lambda)|^2 = 0$ is nearly zero. Here, scattering parameter S_{21} is the transmission at port 2 given incidence at port 1. Then the absorption calculated as A(λ) = 1 - R(λ), where $R(\lambda) = |S_{11}(\lambda)|^2$ is normalized reflected power. Here, scattering parameter S_{11} is the reflection at port 1 given incidence at port 1. In order to achieve a high absorption A(λ) low reflectance R(λ) is mandatory. Similarly, as the absorption in PMA varies with frequency, therefore in order to investigate the absorption performance of absorptivity we describe a Relative Absorption Bandwidth (RAB) parameter as follows:

$$\mathrm{W}_{\mathrm{RAB}}(\lambda) = 2(\lambda_{\mathrm{large}} - \lambda_{\mathrm{short}}) / (\lambda_{\mathrm{large}} + \lambda_{\mathrm{short}}) \times 100$$

2

where λ_{large} and λ_{short} are the large and short wavelength range having absorption A(λ) over 90%, respectively.

Similarly, an overall relative spectral absorption ({I}_{abs}) ratio can be calculated by integrating absorption A(λ) over range of wavelength {\Delta }{\lambda }={{\lambda }}_{2}-{{\lambda }}_{1}.

{\text{I}}_{abs}=\frac{{\int }_{{{\lambda }}_{1}}^{{{\lambda }}_{2}}\text{A}\left({\lambda }\right) \text{d}{\lambda } }{{\Delta }{\lambda }}

Result And Discussions

At the outset, we simulate the absorber for dimension such as thickness t_d = 10 nm, t_m = 10 nm, period P =100 nm, width W_l = 90 nm, W_t = 50 nm, and for 5 metallic layers (each metal layer is separated by dielectric spacer as shown in Fig. 1). The simulated reflection spectra are demonstrated in Fig. 2. The designed PMA illustrates the weakest reflection (10%) around resonant wavelength λ_0 = 1000 nm. Since the ground is made of homogenous metal, the transmission is nearly zero in the entire considered frequency range. In addition, Fig. 3(a)-(b) provides the electric field distribution on the surface of gold layers at 1000 nm wavelength having strong intensity surrounding the top layers of the pyramid. Similarly, Fig. 3(c)-(d) provides the normalized electric field distribution at 500 nm wavelength having highest intensity around top layer.

In this section we analyze the absorption characteristics due to variation in geometric parameters and resonance interference due to multilayer structure. The geometric parameters of PMA contribute to the absorption properties. To analyze the evolution of multilayer PMA we first evaluate the response of single layer absorber. We examine the impact of changing the number of composite layers at fixed height of the pyramid.

Starting from single metallic-dielectric layer to five multilayers using fixed parameters i.e., t_m = t_d =10 nm, and W_t = 50 nm / W_l =90 nm. Figure 3(a) clearly shows that multilayers contribute significantly to overall absorption properties. Absorption due to single layer design remains less than 10% throughout spectrum therefore, W_{RAB} = 0. For 2-layers design results in strong absorption (over 50%) around resonant wavelength λ_0 = 1000 nm and W_{RAB} = 6.58%. Similarly, for 3-layer pyramid design results in strong absorption (over 50%) along with large bandwidth, however resonant wavelength shifted to λ_0 = 900 nm and W_{RAB} = 10.67%. For 4-layers pyramid

design results in overall weaker absorption and W_{RAB} = 8.67%. Finally, 5-layers pyramid design results in multiple bands of strong and weak absorption (over 50%) around λ_0 = 1000 nm and λ_1 = 650 nm wavelength respectively. It is clear from Fig. 4(a) that 5-layer PMA structure has the best absorption bandwidth. In addition, several resonances exist that contributes to overall wideband absorption characteristics. The variation in the absorption spectra shows that the broadband absorption is attributed to the combination of many adjacent resonant absorption peaks. Further layers can be added on top of fifth layer, however we restrict to five multilayers in the current PMA design.

Resonance interference can also be controlled by relative width of adjacent patch layers. To demonstrate the effect on absorption due to width of adjacent layers we define ratio between W_t / W_l. For this purpose, the width of the 5-layer PMA structure is varied in the following. Figure 4(b) shows the corresponding simulated absorption spectra effects for parameter W_t / W_l = 1, 0.75, 0.56, 0.5 and 0.25 respectively.

Table 1
Comparison between bandwidth of 50% and 90% absorption wavelength for varying ratio W_t / W_l.

Type (nm)	50% Absorption Threshold		90% Absorption Threshold		Spectral Absorption ({\text{l}}_{abs})
	Range of wavelength (nm)	W_{RAB}	Range of wavelength (nm)	W_{RAB}	
W_t / W_L = 1	0	0	0	0	38.29%
W_t / W_L= 0.75	0	0	0	0	47.19%
W_t / W_L = 0.56	652 – 561 = 91 965.4 – 668.1 = 297.3	15 36.4	1200 – 1126 = 74	6.36	52.60%
W_t / W_L= 0.5	687.1 – 648.1 = 39 845 – 784 = 61 1012.5 – 932.2 = 80.3	5.84 7.49 8.26	983.8 – 973 = 10.8	1.1	54.06%
W_t / W_L= 0.25	500 – 400 = 100 893 - 598 = 295 1029 – 1001 = 28	22.2 39.6 2.8	707 - 690 = 17 865 – 840 = 25	2.4 3	52.45%

It can be observed that as the ratio W_t / W_l is reduced, the bandwidth of absorption increases due to resonance interference coupling becoming strong. The optimized absorption of the incident wave takes place at the ratio 0.25. Furthermore, overall spectral absorption ({l}_{abs}) reaches 54.06% for W_t / W_L= 0.5. The reason behind the strong resonance interference leading to broadband absorption is resonant detuning effect due to relative change in width (W_t / W_l) of adjacent layers. Such spectral detuning of resonances contributed from adjacent layers allows an overall wideband absorption support for PMA structure.

The absorption spectrum using five multilayers of metal/dielectric material at (W_t / W_l = 0.25) can be further optimized. Keeping all other parameters fixed, the thickness of dielectric patches (i.e., t_d =10 nm, 20 nm, 30 nm) is varied, while thickness of metallic patches t_m keeps constant at 10 nm shown in Fig. 4(c). Similarly, thickness of metal layers (i.e., t_m =10 nm, 20 nm, 30 nm) is varied, while thickness of

dielectric layer t_d is fixed at 10 nm shown at Fig. 4(d). A comparison between relative absorption bandwidths of absorption for the various ratios (Wt / W_l) is provided in Table 2.

Table 2
Comparison between bandwidths & W_{RAB} of 50% and 90% absorption in case of changing t_d and t_m.

Type (nm)	50% Absorption Threshold		90% Absorption Threshold		Spectral Absorption ({\text{l}}_{abs})
	Range of wavelength (nm)	W_{RAB}	Range of wavelength (nm)	W_{RAB}	
$t_d = t_m$ =10	500 – 400 = 100	22.2	707 - 690 = 17	2.4	52.45%
	893 - 598 = 295	39.6	865 – 840 = 25	3	
	1029 – 1001 = 28	2.8			
t_d = 20	932 - 400 = 532	79.9	703 - 652 = 51	7.5	67.2%
t_m= 10	1049 – 992 = 57	5.6	786 -773 = 13	1.7	
			885 - 858 = 27	3.1	
t_d = 30	1025 - 400 = 625	87.7	675 – 644 = 31	4.7	71.1%
t_m= 10	1137 – 1112 = 25	2.2	972 - 930 = 42	4.4	
t_d = 10	956 - 400 = 556	82	500 – 900 = 100	14.3	73.7%
t_m= 20	1060 - 1010 = 50	4.8	656 - 625 = 31	4.8	
			746 – 680 = 66	9.3	
t_d = 10	1029 – 400 = 629	88	570 - 400 = 170	35	76.7%
t_m= 30			640 – 622 = 18	2.9	
			712- 680 = 32	4.6	
			990 – 949 = 41	4.2	

It can be noted that the optimized absorption is at t_d = 10 nm, t_m = 30 nm, where W_{RAB} (above 50%) absorption reaches approximately 88 and W_{RAB} (above 90%) absorption reaches around 35 making the absorber appropriate for practical applications. Furthermore, spectral absorption reaches 76.7% between 400 nm – 1500 nm range of wavelength.

The absorption spectrum can be further optimized by scaling the period (P) of the unit cell. We choose best result achieved using dielectric width t_d = 10 nm and metallic width t_m = 30nm. The period (P) along with all the geometrical parameters are either scaled down by 50% or scaled up by 150%.

In order strong absorption (over 90%) we make the scale down and scale up the whole PMA unit cell structure to half (50% P) and one and half (150% P) respectively. Figure 5 shows that the absorption for

the original structure (i.e., 100% P) exhibits two absorption peaks above 90% absorption. Furthermore, by scaling up the period and the corresponding geometrical parameters of PMA structure (at 150% P) achieves optimized absorption performance. The comparison for scaling the geometrical parameter (P) is provided in Table 3.

Table 3
Comparison between bandwidths & W_{RAB} of 50% and 90% absorption in case of scaling up or scaling down of unit cell of PMA structure.

Type	90% Absorption Threshold		50% Absorption Threshold		Spectral Absorption ({\text{l}}_{abs})
	Range of wavelength (nm)	W_{RAB}	Range of wavelength (nm)	W_{RAB}	
50% P	795 – 400 = 595	85.6	718 – 698 = 20	2.8	52.18%
100% P	1029 – 400 = 629	88	570 - 400 = 170	35	76.8%
			640 – 622 = 18	2.9	
			712- 680 = 32	4.6	
			990 – 949 = 41	4.2	
150% P	705 – 680 = 25	3.76	1171 – 400 = 771	98.15	76.7%
	546.8 – 400 = 148.6	5.04			

It can be observed that scaling down the structure to 50% P the overall spectral absorption ({\text{l}}_{abs}) reduces to 52.18 %. n comparison, the overall spectral absorption ({\text{l}}_{abs}) of 100% P and 150% P reach ~76 %. Also the best absorption of EM takes place at 700 nm and 1000 nm reaches to approximately 96.64% and 99.93%. The increase in absorption with the relatively wider unicell period is attributed to expanded total cross-sectional area covered by the absorber multilayers.

Conclusion

In conclusion, a pyramid metamaterial absorber PMA is simulated to optimize absorption over wideband of optical frequencies. The PMA achieves near- perfect absorption (over 90% threshold) for broad range of visible and infrared frequencies. Various geometrical parameters of the pyramidal structure are varied to achieve an overall optimized design capable to perfectly absorb light along with high spectral absorption ({l}_{abs}) performance. The proposed pyramid metamaterial absorber offers potential applications in stealth technology, antennas, and solar cell technology. On other hand, sharp narrow band absorption peaks can be utilized for sensing applications.

Declarations

Conflict of Interest

The authors declare that they have no conflict of interest.

References

1. T. Ruck, D. E. Barrick, W. D. Stuart, Radar Cross Section Handbook, Vol. 2, Plenum, New York 1970 .
2. Watts, Claire M., Xianliang Liu, and Willie J. Padilla. "Metamaterial electromagnetic wave absorbers." Advanced materials 24.23 (2012): OP98-OP120.
3. Ramzan, Rashad, et al. "Electromagnetically Induced Absorption in the Near-Field of Microwave Radiative Elements With Application to Foliage Moisture Sensing." IEEE Access 6 (2018): 77859–77868.
4. Amin, Muhammad, Mohamed Farhat, and Hakan Bağcı. "An ultra-broadband multilayered graphene absorber." Optics express 21.24 (2013): 29938–29948.
5. B. A. Munk, Frequency Selective Surfaces, John Wiley & Sons, New York 2000.
6. W. W. Salisbury, US Patent 1952 2599944.
7. E. Popov, D. Maystre, R. C. McPhedran, M. Nevière, M. C. Hutley, G.H Derrick, Opt. Exp. 2008, 16, 6146.
8. Khan, Adnan Daud, and Muhammad Amin. "Tunable salisbury screen absorber using square lattice of plasmonic nanodisk." Plasmonics 12.2 (2017): 257-262.
9. Urbas, Augustine M., et al. "Roadmap on optical metamaterials." Journal of Optics 18.9 (2016): 093005.
10. Pendry, John B., et al. "Extremely low frequency plasmons in metallic mesostructures." Physical review letters 76.25 (1996): 4773.
11. Shelby, Richard A., David R. Smith, and Seldon Schultz. "Experimental verification of a negative index of refraction." science 292.5514 (2001): 77–79.
12. Amin, Muhammad, and Adnan D. Khan. "Polarization selective electromagnetic-induced transparency in the disordered plasmonic quasicrystal structure." The Journal of Physical Chemistry C 119.37 (2015): 21633–21638.
13. Amin, M., Mohamed Farhat, and H. Bağcı. "A dynamically reconfigurable Fano metamaterial through graphene tuning for switching and sensing applications." Scientific reports 3 (2013): 2105.
14. Pendry, John Brian. "Negative refraction makes a perfect lens." Physical review letters 85.18 (2000): 3966.
15. Amin, M., et al. "A perfect Fresnel acoustic reflector implemented by a Fano-resonant metascreen." Journal of Applied Physics 123.14 (2018): 144502.
16. Amin, Muhammad, Omar Siddiqui, and Farooq A. Tahir. "Quasi-Crystal Metasurface for Simultaneous Half-and Quarter-Wave Plate Operation." Scientific reports 8.1 (2018): 15743.
17. Meraj-e-Mustafa, H. Farooq, M. Amin, O. Siddiqui, Comment on “A novel ultrathin and broadband microwave metamaterial absorber” [J. Appl. Phys. 116, 094504 (2014)], Journal of Applied Physics 124, 146101, 2018.

18. Amin, M., et al. "Resonant Beam Steering and Carpet Cloaking Using an Acoustic Transformational Metascreen." Physical Review Applied 10.6 (2018): 064030.
19. Pendry, John B., David Schurig, and David R. Smith. "Controlling electromagnetic fields." science 312.5781 (2006): 1780–1782.
20. Amin, Muhammad, Rashad Ramzan, and Omar Siddiqui. "Fano resonance based ultra high-contrast electromagnetic switch." Applied Physics Letters 110.18 (2017): 181904.
21. Amin, Muhammad, Mohamed Farhat, and Hakan Bağcı. "A nonlinear plasmonic resonator for three-state all-optical switching." Optics express 22.6 (2014): 6966–6975.
22. Mandal, P., and S. Sharma. "Progress in plasmonic solar cell efficiency improvement: A status review." Renewable and Sustainable Energy Reviews 65 (2016): 537–552.
23. Zhao, Fangyuan, et al. "Design of plasmonic perfect absorbers for quantum-well infrared photodetection." Plasmonics 9.6 (2014): 1397-1400.
24. Smith, David R., and John B. Pendry. "Homogenization of metamaterials by field averaging." JOSA B 23.3 (2006): 391–403.
25. Li, Wei, and Jason Valentine. "Metamaterial perfect absorber based hot electron photodetection." Nano letters 14.6 (2014): 3510–3514.
26. Zheludev, Nikolay I. "The road ahead for metamaterials." Science 328.5978 (2010): 582–583.
27. Landy, N. Iê¬, et al. "Perfect metamaterial absorber." Physical review letters 100.20 (2008): 207402.
28. Tao, Hu, et al. "A metamaterial absorber for the terahertz regime: design, fabrication and characterization." Optics express 16.10 (2008): 7181–7188.
29. El-Aasser, Mostafa A. "Design optimization of nanostrip metamaterial perfect absorbers." Journal of Nanophotonics 8.1 (2014): 083085.
30. Hedayati, Mehdi Keshavarz, et al. "Design of a perfect black absorber at visible frequencies using plasmonic metamaterials." Advanced Materials 23.45 (2011): 5410–5414.
31. Lin, Chia-Hung, Ruey-Lin Chern, and Hoang-Yan Lin. "Polarization-independent broad-band nearly perfect absorbers in the visible regime." Optics express 19.2 (2011): 415–424.
32. Ye, Yu Qian, Yi Jin, and Sailing He. "Omnidirectional, polarization-insensitive and broadband thin absorber in the terahertz regime." JOSA B 27.3 (2010): 498–504.
33. Hao, Jiaming, et al. "High performance optical absorber based on a plasmonic metamaterial." Applied Physics Letters 96.25 (2010): 251104.
34. Peng, Xiao-Yu, et al. "Ultrathin multi-band planar metamaterial absorber based on standing wave resonances." Optics express 20.25 (2012): 27756–27765.
35. A. T. Mecherikunnel and J. C. Richmond. "Spectral Distribution of Solar Radiation". Technical Memorandum 82021(NASA-TM-82021).
36. Australian Glass And Glazing Association (Agga). " Solar Spectrum ". AGGA Technical Fact Sheet 2018.
37. Butcher, Ginger. Tour of the electromagnetic spectrum. Government Printing Office, 2016.

38. Johnson, P. B. "PB Johnson and RW Christy, Phys. Rev. B 6, 4370 (1972)." Phys. Rev. B 6 (1972): 4370.
39. Amin, M. “Nanoplasmonic Light Trapping Metascreen Encompassing Spectrally Dense Region of Solar Spectrum.” Plasmonics 15, 861–867 (2020).

Figures

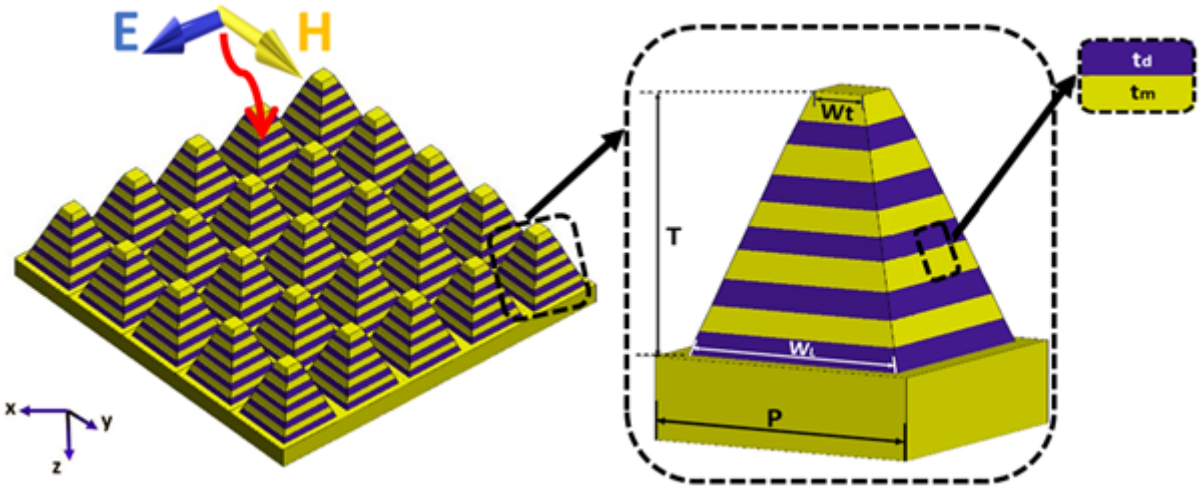

Figure 1

Three-dimensional illustration of the pyramid metamaterial absorber array including the schematic of unit cell. The dimensions of unit cell are W_t = 50 nm, W_l = 90 nm, P = 100 nm, T = 100 nm, T_m = 10 nm, and t_d = 10 nm, where subscripts "m" represents thickness of metal, and "d" for dielectric layers.

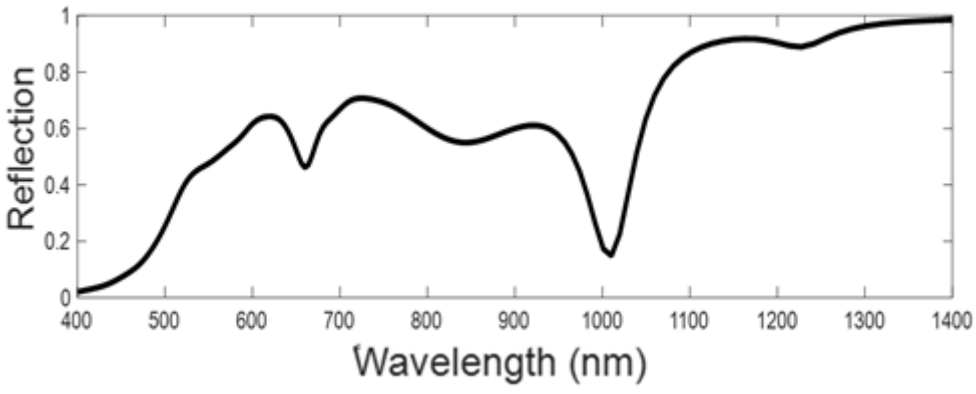

Figure 2

The simulated reflection spectra of the designed PMA shown in Fig. 1

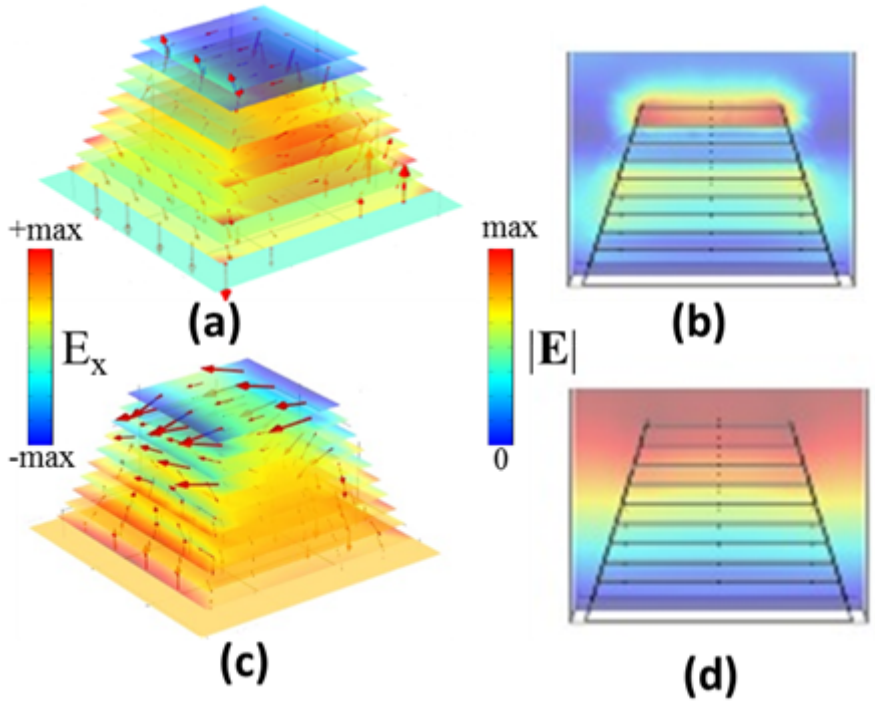

Figure 3

The electric field distribution of the designed PMA shown in Fig. 1 at specific wavelength. (a) the electric field (x-component) distribution on the surface of gold layers (b) normalized electric field along cross-section of pyramid at 1000 nm wavelength. (c) the electric field distribution on the surfaces of gold layers and (d) normalized electric field along cross-section of pyramid at 500 nm wavelength. Corresponding color bars are provided in inset for reference.

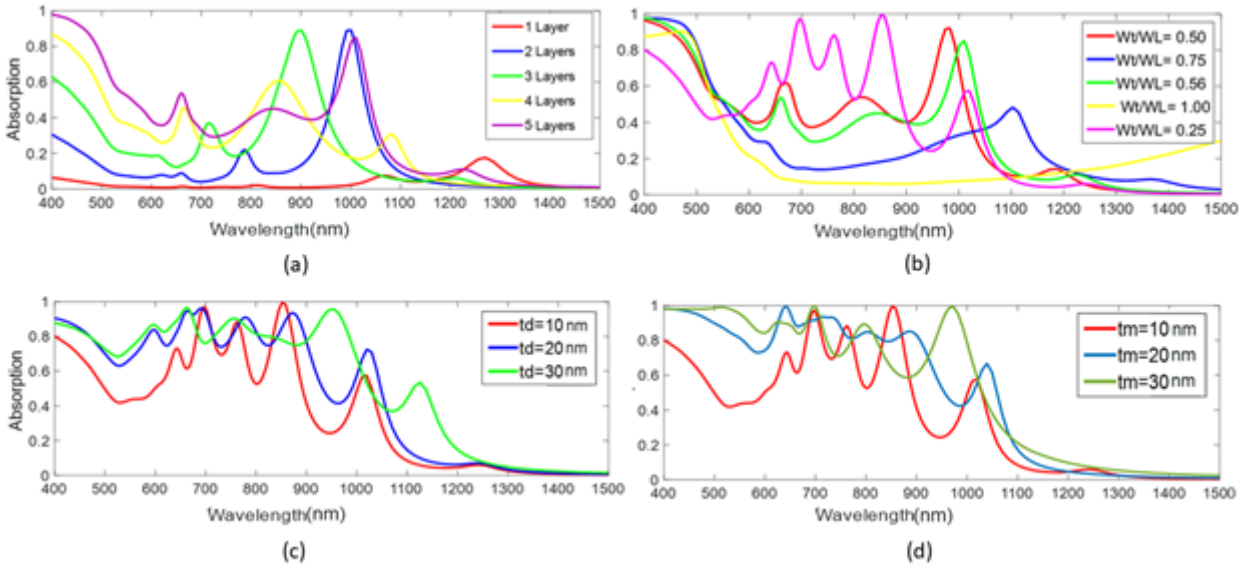

Figure 4

Effect of change in design parameters on the absorption characteristics of the PMA array. (a) Simulated absorption when the number of layers' changes from one to five. (b) Absorption when ratio of the top and

bottom width W_t / W_l changes to 1, 0.75, 0.56, 0.5, and 0.25. (c) Absorption when the fixed t_m = 10 nm and t_d changes from 10 nm to 30 nm. (d) Simulated absorption when the fixed t_d = 10 nm and t_m changes from 10nm to 30nm.

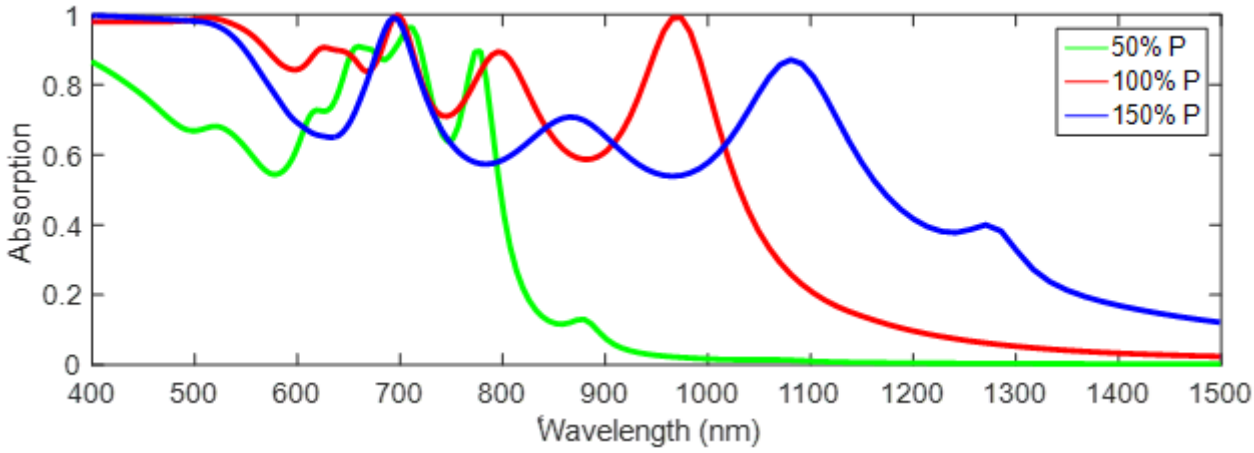

Figure 5

Absorption spectra of the multilayered metallic-dielectric quadrangular frustum pyramids due to variation in PMA structure from P = 100% to P = 50% and P = 150% at fixed number of composite layers, W_t / W_l = 0.25 and t_m = 30 nm.